

Visible Light Induced Photodegradation of Methylene Blue Dye Over ZnO Modified α -Fe₂O₃ Nanocomposites

Abstract

The present investigation aimed to synthesize Zinc (Zn) modified hematite (α -Fe₂O₃) nanocomposites with varying concentrations (pure, 10 wt%, 15 wt%, and 20 wt%) via the modified sol-gel method. The influence of dopants on structural and optical properties and photocatalytic activity of hematite was studied. The X-ray diffraction (XRD) pattern of synthesized samples was indexed to rhombohedral hematite with a crystallite size of 15–25 nm. Moreover, these materials were characterized by FTIR spectroscopy and scanning electron microscopy (SEM). The surface morphology of prepared nanoparticles was explored using scanning electron microscopy (SEM). The specific surface area of the solids was calculated by Brunauer–Emmett–Teller (BET) method. Photocatalytic properties of nanoparticles were performed for methylene blue (MB) dye and showed effective degradation in the presence of UV light. Hence, Zn²⁺ doped hematite can be considered an efficient material for potential applications as a photocatalyst. Zn-doped hematite is developed as a superior photocatalyst for the degradation of MB dye in the presence of UV light.

Keywords: α -Fe₂O₃; Zn-doped α -Fe₂O₃; Nanocomposites; Photodegradation;

1. Introduction

“Photocatalytic degradation of organic dyes in wastewater using metal oxide semiconductors has been considered one of the most promising approaches to solving environmental pollution problems [1-5]. Significantly, metal oxide semiconductors (like TiO_2 , ZnO , Nb_2O_5 , WO_3 , Fe_2O_3 , etc.) have been investigated as photocatalysts due to their potential characteristics, including high degradation efficiency, environment-friendly, thermal stability, abundance, environment-friendly, recyclable visible-light photocatalysis and low-cost products” [6-12].

“Ferrous oxide (Fe_2O_3) appears in four crystallographic phases, namely hematite ($\alpha\text{-Fe}_2\text{O}_3$), maghemite ($\gamma\text{-Fe}_2\text{O}_3$), $\beta\text{-Fe}_2\text{O}_3$, and $\epsilon\text{-Fe}_2\text{O}_3$. The thermodynamically stable hematite phase of Fe_2O_3 is a functional semiconductor with a bandgap of 2.1 eV which is environmentally friendly, non-toxic, and important in various fields. Among them, hematite ($\alpha\text{-Fe}_2\text{O}_3$) has been investigated extensively because it possesses many attractive features, such as ease in handling, chemical stability, nontoxicity, an environment-friendly product, high resistance to corrosion features, and the most stable iron oxide under ambient conditions” [13-15]. “The $\alpha\text{-Fe}_2\text{O}_3$ can absorb visible light since it has a narrow bandgap ($E_g \approx 2.1$ eV) compared to TiO_2 , ZnO , and WO_3 materials. Hematite is a widely investigated material due to its various applications in the fields of photocatalysts, pigments, gas sensors, solar cells, electrochemical sensors, lithium-ion batteries etc. Since the structural and crystallographic forms are generally responsible for their properties, many methods for the synthesis of $\alpha\text{-Fe}_2\text{O}_3$ including hydrothermal synthesis, forced hydrolysis, combustion method, microwave irradiation method, spray pyrolysis, chemical vapor deposition, pulsed laser deposition, co-precipitation, and high

vacuum evaporation and sol-gel is mainly interesting method due to its low cost, high purity, short preparation time, homogeneous solution of doping element and magnify the excellent polycrystalline samples. By doping different metal oxides, it will amplify to find new applications and improve the performance of any other applications. Many researchers have focused on developing mixed oxide semiconductors due to an efficient charge separation obtained by coupling two semiconductor particles with different energy levels” [16-19].“The improvement in the efficiency of photocatalytic reactions is explained as the result of a vectorial transfer of photo-generated electrons and holes from one semiconductor to another” [20, 21]. “Zn-doped hematite materials were synthesized using a modified sol-gel method. ZnO possesses electronic properties and a bandgap energy that is similar to that of TiO₂. It has been reported to be more efficient than TiO₂ in the photooxidation of pollutants”[22, 23].

“The photocatalytic activity of metal oxides depends on the preparation method, which affects the physicochemical properties of the solids. The sol-gel method is a convenient approach for tailoring transition metal oxides for specific applications. The sol-gel method offers the advantage of achieving homogeneous mixing of transition metal cations at the molecular level. This enhances the formation of polycrystalline particles with unique properties” [24]. In this study, we synthesized and characterized mixed photocatalyst Zn-doped α -Fe₂O₃ nanocomposites with varying concentrations (pure, 10, 15, and 20 wt%) using a modified sol-gel method. We evaluated the activities of the catalysts by testing their effectiveness in the photocatalytic degradation of MB dye in aqueous solutions.

2 Materials and Methods

2.1 Materials

Zinc-doped α -Fe₂O₃ nanoparticles were synthesized using reagents without any purification. The precursors used were Fe(NO₃)₃·9H₂O and Zn(NO₃)₂·6H₂O in stoichiometric ratios. Diethylamine was used as a reagent, and saturated ammonia solution was used as a precipitating agent. Double-distilled water was used as the reaction medium.

2.2 Synthesis of pure and Zn doped α -Fe₂O₃ nanoparticles

An aqueous solution containing iron nitrate and zinc nitrate at specified weight ratios (10:90, 15:85, and 20:80) was prepared by dissolving them in 100 ml of double distilled water. The mixture underwent magnetic stirring for 4 hours. Diethylamine was then added to the solution, followed by continued stirring for an additional 2 hours. A saturated solution of ammonium hydroxide was subsequently introduced, and the mixture was stirred at 75°C for another 2 hours, resulting in the formation of a brown-colored solution. After filtration, the solution was thoroughly washed with water and ethanol. The filtered material was dried at 350°C in an oven to yield a gel, which was further subjected to calcination at 450°C and 500°C for 3 hours each.

2.3 Characterization

The synthesized nanocomposites underwent characterization using various spectroscopic techniques such as X-ray diffraction (XRD), Fourier Transform Infrared Spectroscopy (FTIR), scanning electron microscopy (SEM), and UV-visible spectroscopy. The surface area and pore size were determined

by analyzing the N₂ adsorption-desorption isotherm and BJH method using a Micromeritics Analyzer (ASAP 2460) at 77 K.

A series of experiments were conducted to evaluate the photocatalytic degradation of MB dye using a photoreactor under UV light irradiation. The light source utilized for photocatalysis was visible light (40 W Hg lamp). After the photocatalytic process, the catalysts and solution were separated via filtration, and the collected samples were analyzed using a UV-Vis spectrophotometer (Shimadzu UV-2450).

The efficiency of photodegradation for RB5 was determined using the following formula:

$$\% \text{ Degradation efficiency} = \frac{C_o - C_t}{C_o} \times 100$$

Where, C_o is the original MB dye concentration, C_t is the retained MB dye concentration.

3. Result and discussion

3.1 X-ray diffraction

The structural analysis and phase identification of synthesized materials were verified using X-ray diffraction (XRD) technique and presented in Figure 1. Only hematite diffraction peaks were observed, indicating that zinc atoms were successfully incorporated into the Fe₂O₃ matrix. This incorporation did not disrupt the rhombohedral structure of hematite, demonstrating that the dopant atoms altered the crystallinity.

The crystal structure of the zinc-doped hematite nanocomposites was determined and confirmed using an X-ray diffraction meter (Model Miniflex 600,

RIGAKU, Japan) with Cu K α radiation ($\lambda = 1.5405 \text{ \AA}$) across a wide range of Bragg angles. The crystalline size was calculated based on the peak widths of the XRD patterns, ensuring minimal non-uniform strains. The particle size of the synthesized samples was estimated using Scherrer's equation [24], which is formulated as:

$$D = \frac{0.95\lambda}{\beta \cos\theta}$$

where λ is the X-ray wavelength, β is the full width at half maximum (FWHM) and θ is the diffraction angle, D is the average crystalline size perpendicular to the reflecting angle.

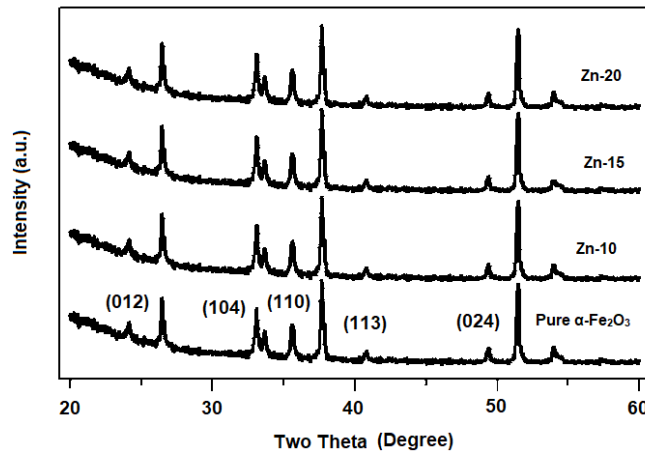


Figure 1. XRD pattern of pure and Zn doped α -Fe $_2$ O $_3$ materials.

The peaks at 2θ values of 24.27, 33.34, 35.80, 41.00, 49.64, 54.18, 62.66, and 64.17 correspond to the lattice planes (012), (104), (110), (113), (024), (116), (214), and (300) respectively. These peaks indicate that the synthesized nanoparticles are in the hematite phase with a rhombohedral structure, as confirmed by JCPDS card No. 89-8104. The average crystallite size of the nanoparticles was estimated using the Debye-Scherrer equation and found to be 35 ± 20 nm. Additionally, a secondary phase corresponding to the

(110) plane confirms the incorporation of Zn into the Fe_2O_3 lattice. When the zinc content was increased to 15%, the crystallinity of synthesized materials decreased, suggesting that more strain was introduced into the Fe_2O_3 lattice.

3.2 Scanning electron microscopy (SEM)

Figure 2 shows the SEM micrographs of Zn-doped samples, revealing cluster formations with crystalline characteristics. The images depict spherical structures ranging in size from 15 to 35 nm with irregular surface morphologies. The stony appearance is likely due to the aggregation of nanoparticles.

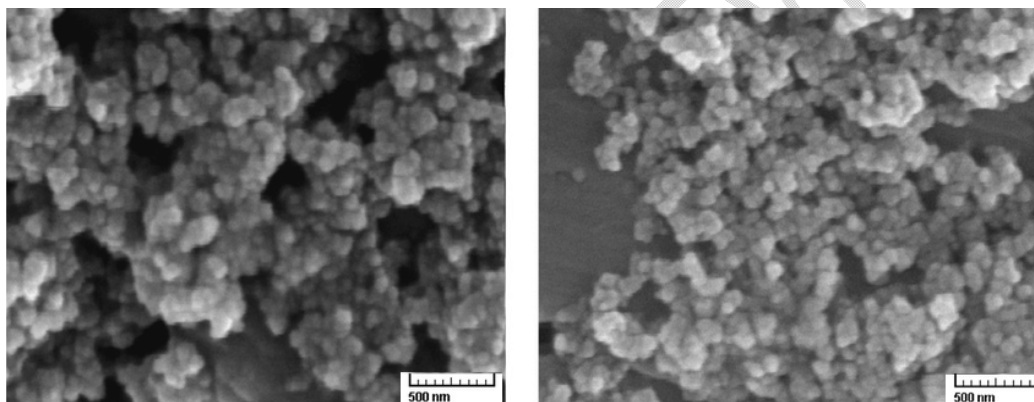


Figure 2 SEM images of Zn-doped samples.

3.3 FT-IR Studies

The presence of functional groups adsorbed on the surface of synthesized pure and Zn-doped hematite nanocomposites was determined using FT-IR spectroscopy. The FT-IR spectra of pure Zn-doped hematite calcined at 550°C are shown in Figure 3. As depicted in Figure 3, distinctive bands are observed at 3446 , 1642 , 571 , and 478 cm^{-1} . The characteristic Fe-O peaks appear sharply at 478 and 571 cm^{-1} , while the broadband at 3446 cm^{-1} corresponds to the O-H stretch of water molecules. In the regions around 3430

cm^{-1} and 1639 cm^{-1} , observed absorption bands are attributed to the stretching and bending vibrations of water molecules. The bands at 571 cm^{-1} and 478 cm^{-1} are caused by the presence of the dopant and the Fe-O vibrational mode of hematite nanoparticles, confirming the hematite phase in the rhombohedral lattice.

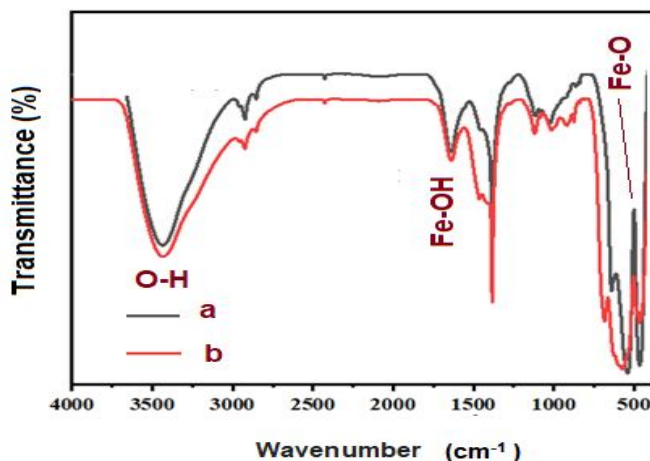


Figure 3 FT-IR spectra of (a) pure $\alpha\text{-Fe}_2\text{O}_3$ and (b) Zn-15 sample.

3.4 UV-Vis absorption spectrum

The size of particles significantly affects the properties of nanomaterials. Therefore, monitoring the size evolution of semiconducting nanoparticles is crucial for understanding their properties. UV-visible absorption spectroscopy is a commonly used technique for analyzing the optical properties of nanosized particles. Figure 4 presents the absorption spectra of pure $\alpha\text{-Fe}_2\text{O}_3$ and Zn-doped $\alpha\text{-Fe}_2\text{O}_3$ nanocomposites. As shown in Figure 4, the absorption spectra of synthesized hematite in the UV-Vis range exhibit strong absorption between 500 and 700 nm. This observation is consistent with data reported in other studies [5-7]. The optical bandgap (E_g) of nanoparticles can be assessed by extrapolating from the absorption edge, according to the following equation:

$$(ahv)^n = A (hv - E_g)$$

Where α is the absorption coefficient, A is constant, h is the energy of light and n is a constant depending on the nature of the electron transition.

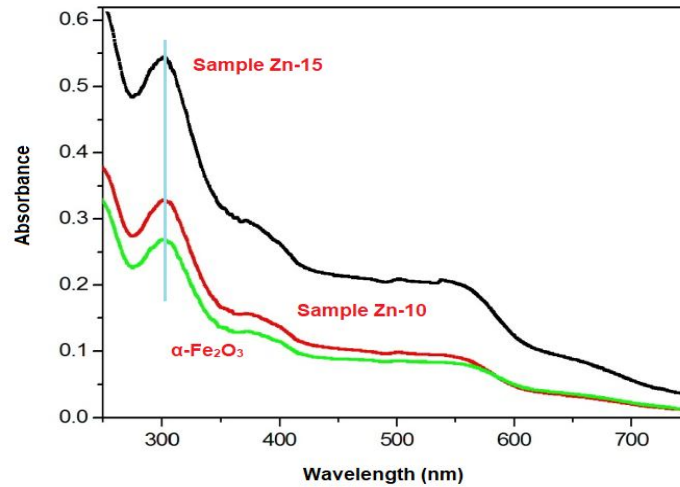


Figure 4 UV-Vis spectra of synthesized pure and Zn-doped Fe₂O₃ samples.

Table 1 Summary of BET-Specific Surface Area, Pore Volume, and Pore Size of the as-synthesized samples.

Sample	BET specific surface area (m ² g ⁻¹)	Pore volume (cm ³ /g)	Pore size (Å)
Pure α-Fe ₂ O ₃	12.523	0.0121	29.2
Zn-10	16.569	0.0132	31.5
Zn-15	34.543	0.0456	42.2
Zn-20	17.459	0.0143	30.4

3.5 BET analysis

The surface areas and porosities of the as-synthesized nanomaterials were quantitatively assessed using nitrogen adsorption BET). Before measuring the N₂ adsorption–desorption isotherms at –196°C, the samples were degassed at 150°C for 45 hours. The Brunauer-Emmett-Teller (BET) surface areas, pore volumes, and pore sizes of the synthesized samples are

detailed in Table 1. Notably, the Zn-doped α -Fe₂O₃ materials exhibited increased surface area, pore volume, and pore size compared to pure α -Fe₂O₃. It is important to highlight that photocatalytic performance is influenced by surface area, pore size, and pore volume; a greater pore volume, porosity, and surface area enhance the catalyst's ability to interact with and adsorb pollutants.

3.6 Photocatalytic studies

Hematite is a semiconductor with a bandgap of 2.0–2.6 eV and can absorb light from the visible to UV regions of the solar spectrum at specific wavelengths [27]. Therefore, the synthesized nanomaterials could serve as efficient photocatalysts for the rapid degradation of dyes. In this study, we evaluated the photocatalytic activity of the prepared nanoparticles under UV light irradiation using a Methylene Blue (MB) aqueous solution as a model contaminant. Methylene Blue dye is odorless, solid at room temperature, and appears as a dark green powder that turns blue when dissolved in water. MB, a Phenothiazine dye, is extensively used in dyeing and printing industries and has severe toxic effects on human health. UV-visible spectroscopy reveals that MB has three absorption maxima at 246 nm, 291 nm, and 663 nm. The absorption maxima at 291 nm and 663 nm are commonly used for the photodegradation of MB dye. The concentration of the MB dye, in terms of absorbance, was measured at 663 nm (λ_{max} for Methylene Blue) before and after photocatalytic degradation. To elucidate the effect of ZnOwt% on the photocatalytic activity of the α -Fe₂O₃ photocatalyst, parallel experiments were conducted with synthesized photocatalysts containing different ZnOwt%. We investigated various operating parameters, such as Zn doping, pH, catalyst

loading, initial dye concentration, oxygen bubbling, and direct solar light, on the photodegradation of MB dye.

The progress of the photocatalytic reaction was monitored by measuring absorbance at regular time intervals. It was found that hematite nanoparticles synthesized with higher dopant concentrations exhibited higher removal efficiencies. The absorbance of MB dye decreased in the presence of the as-synthesized materials and UV light, as shown in Figure 5. The plot of absorbance versus time was linear, indicating that the reaction followed pseudo-first-order kinetics. The pseudo-first-order kinetic equation is presented below:

$$\ln \frac{C_0}{C_t} = kt$$

Where C_0 and C_t are the concentrations of dye in solution at times 0 and t respectively, and k is the first-order rate constant (min^{-1}). It can be predicted from Figure 5, that after 100 minutes maximum degradation of MB dye was achieved for pure $\alpha\text{-Fe}_2\text{O}_3$ sample.

3.6.1 Effect of Zn-doping

The photocatalytic efficiency of Zn-doped $\alpha\text{-Fe}_2\text{O}_3$ photocatalysts depends on their ability to generate $\cdot\text{OH}$ radicals in an aqueous solution under irradiation. The concentration of dopants in host metal oxide influences the production of $\cdot\text{OH}$ radicals. Figure 5 shows that as the Zn concentration increases, the degradation efficiency of MB dye improves over time, with the highest efficiency achieved with Zn-15 in 72 minutes. This indicates that Zn-

doped $\alpha\text{-Fe}_2\text{O}_3$ nanoparticles could be effective photocatalysts for removing methylene blue pollutants from industrial effluents.

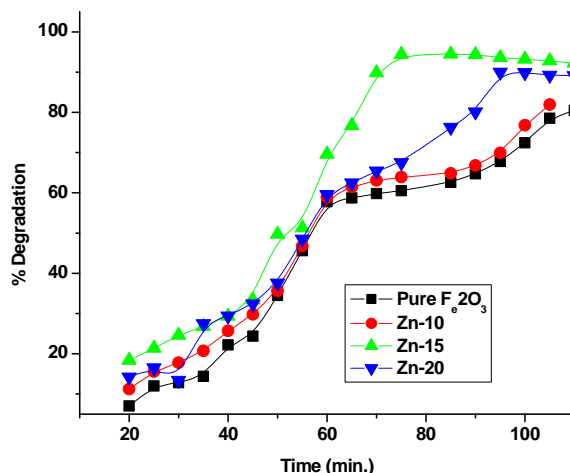


Figure 5 Photodegradation of MB dye using pure and doped α -hematite.

3.6.2 Effect of Catalyst dose

The effect of varying catalyst doses on the photodegradation of MB dye was investigated, with the results shown in Figure 5. In this study, the dose of pure and Zn-doped $\alpha\text{-Fe}_2\text{O}_3$ nanocomposites was varied from 100 to 400 mg/L for an initial dye concentration of 20 mg/L at pH 2, using UV light as the irradiation source. The findings presented in Figure 5 reveal that the degradation percentage increased with catalyst dosage up to a certain point. However, increasing the catalyst dosage beyond this point resulted in a decrease in dye degradation. The most effective catalyst dosage was determined to be 200 mg/L.

The initial increase in percent degradation is likely due to a rise in the number of active sites on the catalyst's surface with a higher catalyst dosage. As the dosage increases, the concentration of free radicals, such as $\bullet\text{OH}$ and

O_2^{2-} , in the solution also rises, enhancing the photodegradation of the wastewater sample [22]. However, additional increases in catalyst dosage resulted in reduced photodegradation due to the excessive amount of catalyst. At this stage, the catalyst particles start to clump together, decreasing the amount of sunlight that reaches the active sites and thus reducing the reaction rate. This finding is consistent with prior research [23-24].

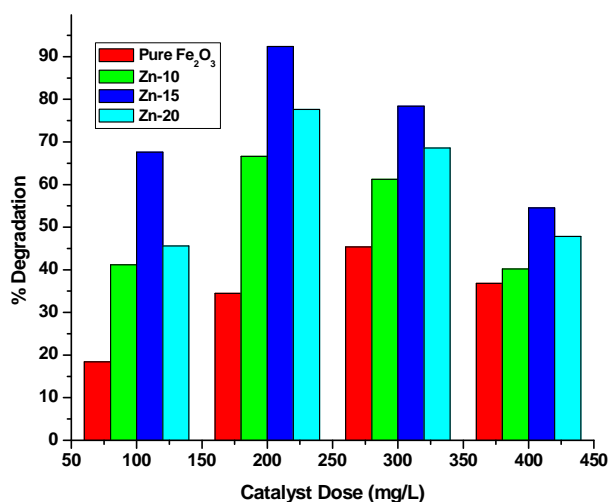


Figure 6 Effect of catalyst dosage on MB dye degradation.

3.6.4 Effect of pH

In photocatalytic studies, pH is essential for controlling the reactions related to the degradation of organic compounds and influences the generation of hydroxyl radicals [20, 21]. Initially, the impact of pH on the photocatalytic degradation of MB dye was investigated across a pH range of 1–10 using the synthesized nanomaterials, with conditions set at a contact time of 120 minutes, a dye concentration of 20 mg/L, and a catalyst dose of 1 g/L, as shown in Figure 7. The pH of the solution influences the surface charge

properties of the catalyst, which in turn affects the adsorption behavior of the photocatalyst [22].

The percentage of dye removal increased as the pH value decreased, peaking in the acidic range at pH 2. At lower pH values, the surfaces of the catalysts became highly protonated and positively charged, which enhanced the electrostatic attraction of dye cations to the catalyst surface. This increase in oxidizing holes resulted in improved degradation of MB dye. In acidic conditions positive holes serve as the primary oxidation species, while hydroxyl radicals are the predominant species at neutral or alkaline pH levels [24]. The maximum degradation of MB dye was achieved at pH 2, with pure $\alpha\text{-Fe}_2\text{O}_3$ and Zn-15 samples showing degradation rates of 74.6% and 92.8%, respectively.

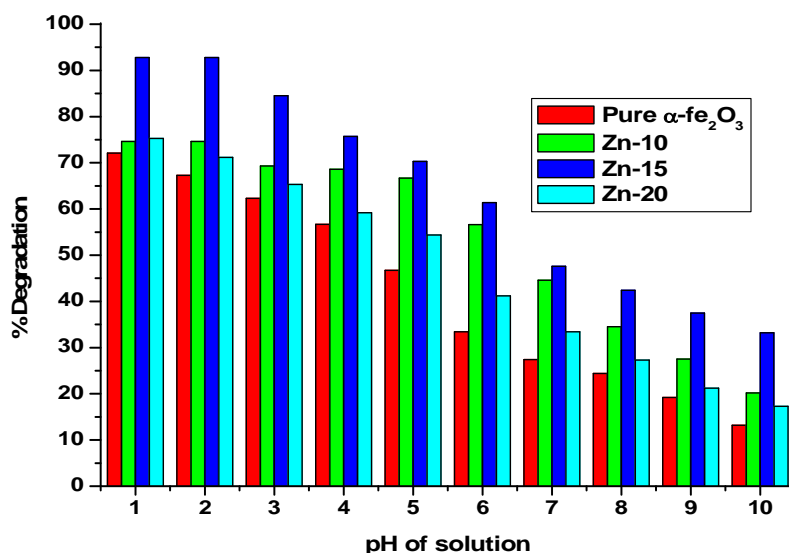


Figure 7 Effect of pH on photodegradation of MB dye.

3.6.5 Effect of initial dye concentration

The impact of initial dye concentration on degradation efficiency was examined at an optimized pH of 2 with a fixed catalyst dose by varying the initial dye concentration. MB dye concentrations ranging from 10 to 50 mg/L were tested to evaluate photocatalytic activity. Figure 8 illustrates that maximum dye degradation occurred at an initial concentration 20 mg/L. It was observed that as the initial dye concentration increased, the degradation efficiency decreased. This is because a higher dye concentration leads to an excess of dye molecules adsorbed onto the catalyst surface, reducing the availability of active sites. As the dye concentration increases, more hydroxyl radicals are required for degradation. However, the production of hydroxyl radicals on the catalyst surface remains constant for a fixed light intensity, catalyst dose, and irradiation time[25]. As a result, at higher dye concentrations, the number of available hydroxyl radicals becomes inadequate for effective degradation, resulting in decreased photodegradation efficiency.

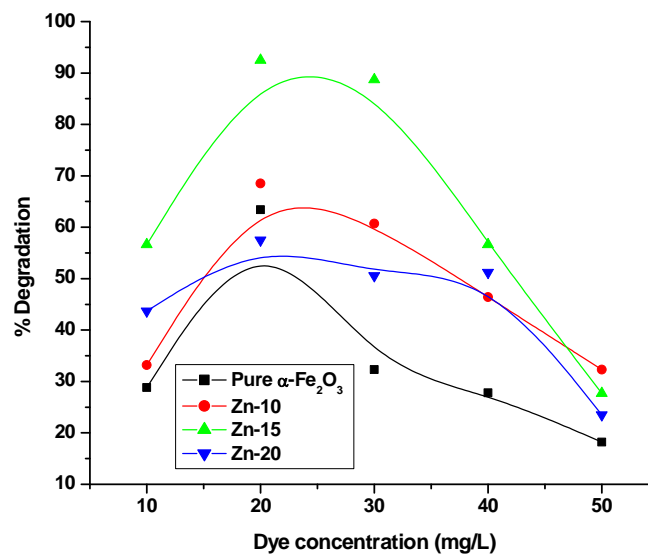


Figure 8 Effect of dye concentration on dye degradation at pH 2.

3.6.6 Effect of bubbling oxygen

To assess the impact of oxygen bubbling on photocatalytic efficiency, MB dye degradation was evaluated by introducing oxygen into an aqueous suspension containing 20 mg/L of dye and 1 g/L of Zn-15 catalyst. Degradation experiments were also performed in a deoxygenated medium by removing oxygen through nitrogen bubbling for 30 minutes, and then sealing the reactor with a septum to prevent external interactions. The results, shown in Figure 9, demonstrate that degradation performance is significantly higher in the oxygenated environment compared to the non-oxygenated medium. Specifically, the degradation yield of MB dye with oxygen was around 98.5%, while it was approximately 92.4% in the absence of oxygen.

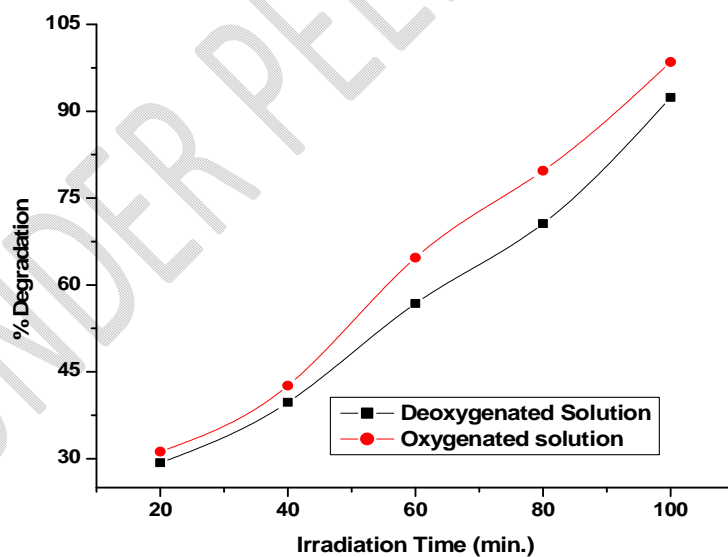


Figure 9 Degradation of MB as a function of irradiation time in oxygenated and deoxygenated aqueous medium.

3.6.7 Solar light photodegradation of MB dye

Solar radiation offers the benefit of being an abundant and environmentally friendly energy source. However, the two photocatalysts absorb only a small fraction of the total sunlight. It is valuable to investigate the photocatalytic degradation of an aerated MB solution with the Zn-15 sample, as shown in Figure 10. For this experiment, we used a similar approach to UV irradiation but exposed the MB dye (20 mg/L) solution directly to solar radiation (sunlight intensity at 355 nm). Photodegradation of MB under direct sunlight began to show progress after 55 minutes of exposure. Due to the substantial amount of light absorbed by the photocatalyst, the degradation process accelerated after 120 minutes.

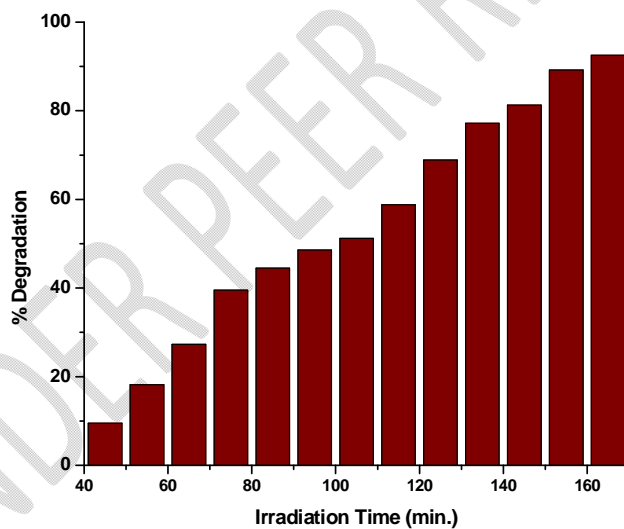


Figure 10 Kinetics of the MB dye (20 mg/L) photocatalytic degradation using sample Zn-15 with solar light irradiation.

3.6.8 Reusability of photocatalyst

Currently, recovery and reusability are crucial factors in choosing a cost-effective and practical catalyst for pilot-scale remediation systems.

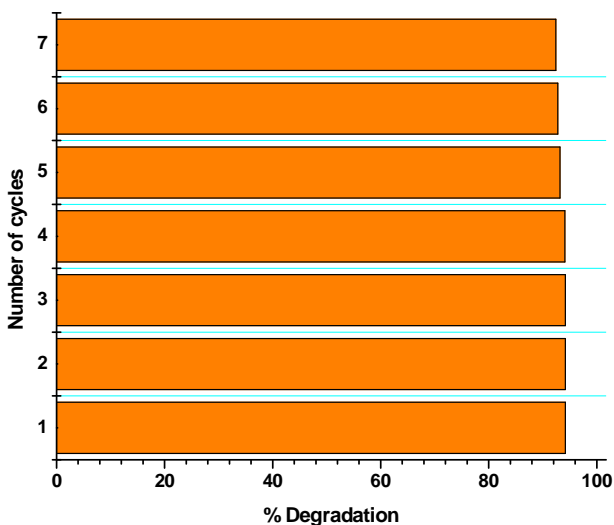


Figure 11 Reusability function of Zn-15 sample for degradation of MB dye.

The reusability of the synthesized nanomaterials was assessed over seven cycles of MB dye photodegradation using 100 mL of a 20 mg/L MB dye solution at pH 2 with a catalyst dose of 1 g/L. Figure 11 shows the recyclability and stability of the Zn-15 catalyst after seven cycles, each lasting 70 minutes. The Zn-15 catalyst was easily recyclable using a strong magnet and could be reused. After seven cycles, the photoactivity of the Zn-15 catalyst declined by 5%, yet it maintained high efficiency. This minor reduction in photocatalytic activity can be attributed to several factors: (i) Material loss during washing and drying led to a reduced dose in subsequent cycles, diminishing surface catalytic activity and overall performance [24]. (ii) Nanoparticle aggregation decreased the effective surface area and the number of active sites, potentially causing

fouling and performance changes over multiple cycles [35]. (iii) The catalyst's surface activity progressively decreased due to the accumulation of catechol and its intermediates, which blocked the pores and active sites after each cycle. [36].

4. Conclusion

In this report, Zn-doped α -Fe₂O₃ nanocomposite is synthesized through a thermal decomposition method and then applied for the photocatalytic degradation of methylene blue (MB) dye. The as-synthesized catalyst was characterized by XRD, revealing that the doped Zn was effectively integrated into the structure. However, a shift in 2θ values towards higher angles was observed. SEM results showed the sphere-shaped morphology of the catalyst in the range of 27-52 nm in size. The surface area of as-synthesized Zn doped α -Fe₂O₃ nanocomposite was found to be 16.569, 34.543, and 17.459 m²/g, and that for pure is 12.523 m²/g through the BET analysis. The Zn-doped α -Fe₂O₃ nanocomposite was found to have an improved degradation efficiency than the catalyst when used under visible light, and it showed about 92.81% degradation of MB dye within 150 minutes. The degradation of MB dye was investigated by varying parameters such as catalyst dose, pH, initial dye concentration, and the introduction of O₂ through bubbling. Then the reusability of the catalyst was studied by performing a cyclic test, and the catalyst showed good photocatalytic activity up to seven consecutive cycles. From the results obtained, we propose a Zn-doped α -Fe₂O₃ nanocomposite as an efficient photocatalyst for the degradation of organic dyes, and it can be applied to other organic pollutants in the future.

Disclaimer (Artificial intelligence)

Option 1:

Author(s) hereby declare that NO generative AI technologies such as Large Language Models (ChatGPT, COPILOT, etc) and text-to-image generators have been used during writing or editing of manuscripts.

Option 2:

Author(s) hereby declare that generative AI technologies such as Large Language Models, etc have been used during writing or editing of manuscripts. This explanation will include the name, version, model, and source of the generative AI technology and as well as all input prompts provided to the generative AI technology

Details of the AI usage are given below:

- 1.
- 2.
- 3.

5. References

[1] Zhang, Y.J. et al. (2015) Alkali-activated cements for photocatalytic degradation of organic dyes. In: *Handbook of Alkali-Activated Cements, Mortars and Concretes*. Elsevier: Amsterdam, p. 729.

[2] Zhang, Y.J. et al. (2013). "A facile and low-cost synthesis of granulated blast furnace slag-based cementitious material coupled with Fe_2O_3 catalyst for treatment of dye wastewater," *Appl. Catal. B*, Vols.138–139, pp. 9–16.

[3] Dutta, A.K., Maji, S.K. & Adhikary, B. (2014) γ - Fe_2O_3 nanoparticles: An easily recoverable effective photo-catalyst for the degradation of rose bengal and

methylene blue dyes in the waste-water treatment plant. *Materials Research Bulletin*, 49, 28–34.

[4] Li, X., Liu, Y., Zhang, C., Wen, T., Zhuang, L., Wang, X., Song, G., Chen, D., Ai, Y., Hayat, T. & Wang, X. (2018) Porous Fe₂O₃ microcubes derived from metal organic frameworks for efficient elimination of organic pollutants and heavy metal ions. *Chemical Engineering Journal*, 336, 241–252.

[5] Guo, S.Q., Hu, Z., Zhen, M., Gu, B., Shen, B. & Dong, F. (2020) Insights for optimum cation defects in photocatalysis: A case study of hematite nanostructures. *Applied Catalysis B*, 264, 118506.

[6] Souza, J.B. (2021) Junior Jr., et al, “On the relevance of understanding and controlling the locations of dopants in hematite photoanodes for low-cost water splitting,”. *Applied Physics Letters*, 119, 200501.

[7] Rasheed, R.T. et al. (2018) Preparation and characterization of hematite iron oxide (α -Fe₂O₃) by sol–gel method. *Chemical Sciences Journal*, 9, 2.

[8] Tsege, E.L., Atabaev, T.S., Hossain, M.A., Lee, D., Kim, H. & Hwang, Y. (2016) Cu-doped flower-like hematite nanostructures for efficient water splitting applications. *Journal of Physics and Chemistry of Solids*, 98, 283–289.

[9] Meng, Q.L., Wang, Z., Chai, X., Weng, Z., Ding, R. & Dong, L. (2016) Fabrication of hematite (α -Fe₂O₃) nanoparticles using electrochemical deposition. *Applied Surface Science*, 368, 303–308.

[10] Cao, Z.Q., Qin, M., Gu, Y., Jia, B., Chen, P. & Qu, X. (2016) Synthesis and characterization of Sn-doped hematite as visible light photocatalyst. *Materials Research Bulletin*, 77, 41–47.

[11] Mahmoodi, N.M. (2013) Photocatalytic degradation of dyes using carbon nanotube and titania nanoparticle. *Water, Air, and Soil Pollution*, 224, 1612.

- [12] Oveisi, M., Mahmoodi, N.M.&Asli, M.A. (2019) Facile and green synthesis of metal–organic framework/inorganic nanofiber using electrospinning for recyclable visible-light photocatalysis.*Journal of Cleaner Production*, 222, 669–684.
- [13] Alagiri, M.&Hamid, S.B.A. (2015) Sol–gel synthesis of α - Fe_2O_3 nanoparticles and its photocatalytic application.*Journal of Sol-Gel Science and Technology*, 74, 783–789.
- [14] Sarkar, D., Mandal, M.&Mandal, K. (2013) Design and synthesis of high performance multifunctional ultrathin hematite nanoribbons.*ACS Applied Materials and Interfaces*, 5, 11995–12004.
- [15] Maji, S.K., Mukherjee, N., Mondal, A.&Adhikary, B. (2012) Synthesis, characterization and photocatalytic activity of α - Fe_2O_3 nanoparticles.*Polyhedron*, 33, 145–149.
- [16] Valenzuela, M.A., Bosch, P., Jiménez-Becerrill, J., Quiroz, O.&Páez, A.I. (2002) Preparation, characterization and photocatalytic activity of ZnO , Fe_2O_3 and ZnFe_2O_4 .*Journal of Photochemistry and Photobiology A*, 148, 177–182.
- [17] SeneJeosadeque, J.et al. (2003).*Journal of Physical Chemistry. Part B*, 107, 1597.
- [18] Chiang, K., Amal, R.&Tran, T. (2002) Photocatalytic degradation of cyanide using titanium dioxide modified with copper oxide.*Advances in Environmental Research*, 6, 471–485.
- [19] Sadeghi, M., Liu, W., Zhang, T., Stavropoulos, P.&Levy, B. (1996) Role of photoinduced charge carrier separation distance in heterogeneous photocatalysis: Oxidative degradation of CH_3OH vapor in contact with Pt/TiO_2 and Cofumed TiO_2 – Fe_2O_3 .*Journal of Physical Chemistry*, 100, 19466–19474.

- [20] Ho, W., Yu, J.C., Lin, J., Yu, J.&Li, P. (2004) Preparation and photocatalytic behavior of MoS₂ and WS₂ nanocluster sensitized TiO₂. *Langmuir*, 20, 5865–5869.
- [21] Serpone, N. (1995) Photochemphotobiol. *Annali di Chimica*, 85, 247.
- [22] Villasenor, J. et al. (1998). *J Chem Technol Biotechnol* ~72 : 105, Vol. 13.
- [23] Pal, B. & Sharon, M. (2002) Enhanced photocatalytic activity of highly porous ZnO thin films prepared by sol–gel process. *Materials Chemistry and Physics*, 76, 82–87.
- [24] Ding, Z., Lu, G.Q. & Greenfield, P.F. (2000) Role of the crystallite phase of TiO₂ in heterogeneous photocatalysis for phenol oxidation in water. *Journal of Physical Chemistry B*, 104, 4815–4820.
- [25] Lalithambika, K.C. et al. (2017). *Journal of Materials Science: Materials in Electronics*, 282062.
- [26] Sherman, D.M. (2005) Electronic structures of iron (III) and manganese (IV) (hydr) oxide minerals: Thermodynamics of photochemical reductive dissolution in aquatic environments. *Geochimica et Cosmochimica Acta*, 69, 3249–3255.
- [27] Marathe, Y.V., Ramanna, M.M.V. & Shrivastava, V.S. (2013) Synthesis and characterization of nanocrystalline CdS thin films grown by chemical bath deposition at different molarities for removal of methylene blue. *Desalination and Water Treatment*, 51, 5813–5820.